RSC Advances

ROYAL SOCIETY OF CHEMISTRY

www.rsc.org/advances

Cite this: DOI: 10.1039/c0xx00000x

www.rsc.org/xxxxxx

ARTICLE TYPE

A Mechanistic Study on the Effect of Surface Protecting Agent on Electrocrystallization of Silver Nanoparticles

Saurav K. Guin, Rohan Phatak, Jisha S. Pillai, Arnab Sarkar and Suresh K. Aggarwal*

Received (in XXX, XXX) Xth XXXXXXXXX 20XX, Accepted Xth XXXXXXXXX 20XX

DOI: 10.1039/b000000x

Cyclic voltammetry and chronoamperometry at characteristic potentials were employed to unravel the mechanism of electrocrystallization of silver nanoparticles (AgNPs) from its aqueous solution in the presence and absence of surface protecting agent tetrabutylammonium tetrafluoroborate ($TBABF_4$). The electrocrystallization parameters viz. initial current density (j_0), decay constant (τ), diffusion coefficient (D) of Ag(I), number of active sites (N_0) and nucleation rate (a) were calculated by fitting the experimentally obtained current transients with the calculated current transients using hybrid genetic algorithm (HGA). The theoretical currents were calculated from three popular electrocrystallization models viz. Scharifker and Mostany (SM); Sluyters-Rehbach, Wijenberg, Bosco and Sluyters (SRWBS) and Heerman and Tarallo (HT). Each of the three models fitted well by HGA with the potentiostatic current transients observed at different potential, both in the absence and in the presence of $TBABF_4$ with residual sum of squares ($\sim10^{-7}$) and reduced χ^2 ($\sim10^{-10}$). However, electrocrystallization parameters were distinctly different in each of the three models. Principal component analysis of the calculated parameters i.e. D, N_S and aN_0 showed the absence of any correlation among the electrocrystallization parameters derived from the Scharifker and Hills (SH), SM, SRWBS and HT models. Further, the actual nuclei densities of the AgNPs, both in the presence and the absence of $TBABF_4$, were found significantly higher than the predicted values from any of these models. Since these models are based on different empirical assumptions, one needs be careful in attaching any extra significance to the numerical values of j_0, τ, D, N_0, "a" of any system only based on the quality of fitting. From the present data, it was conclusively proved that the surface protecting agent slowed down the kinetics of electrocrystallization due to introduction of higher activation overpotential at the electrode-electrolyte interface and subsequently decreases in the number of nuclei on the electrode surface in presence of TBA^+ ions, irrespective of the model.

1. Introduction

Silver nanoparticles (AgNPs) have received considerable attention in the field of catalysis, biological and chemical sensors and Surface-Enhanced Raman Spectroscopy (SERS).[1] The plasmonic resonance and other properties of AgNPs strongly depend on their size, shape and composition.[2-4] However, synthesizing nanoparticles of uniform shapes and monodispersity is still a challenging task, which attracts several researchers worldwide. Surface protecting agents play an important role in controlling the shape and size of NPs. The cationic surfactant, cetyltrimethylammonium bromide (CTAB), is most extensively used as a surface stabilizer to fabricate positively charged bi-layer shell on AgNPs, where CTA^+ ions present in the first layer cap the Ag clusters via their head groups. Methylene chains of the two layers form a bi-layer shell and the head groups of the CTA^+ ions, present in the second layer, are exposed to the solution.[5]

Electrosynthesis is one of the attractive solution based routes for the preparation of metal nanoparticles, because it does not require any additional reducing agents or chemicals during the process. The mechanistic studies on electrocrystallization are important to understand the electrosynthesis of supported metal nanoparticles of controlled size, shape, crystallographic orientation. Guin et al. reported template free electrosynthesis strategies with optimised pulse parameters for achieving controlled particle size dispersion without employing any surface stabilizing agent.[6,7] However, from the application point of view, chemical stability of nascent nanoparticles in aqueous solution is often questioned in absence of any surface stabilising or protecting agent. Here we report the mechanisms of electrocrystallization of Ag from its aqueous solution at selected potentials both in the presence and absence of surface protecting agent tetrabutylammonium tetrafluoroborate ($TBABF_4$). The cyclic voltammetry and chronoamperometry were used to understand the influence of $TBABF_4$ on the formation and growth of silver nuclei on glassy carbon electrode. The other possible counter anions of TBA^+ viz. Br^-, ClO_4^-, PF_6^- etc. were avoided to eliminate any precipitation and decomposition.

The electrocrystallization mechanism can be studied by

various approaches e.g. potentiostatic current transient analysis, computer simulation, scanning probe microscopic observations of electrode surface.[8] The first approach is simple and used more frequently in electrochemistry and was, therefore, also selected for the present study. The electrocrystallization of metal involves nucleation of metal adatoms on the active sites of the electrodes followed by three dimensional diffusion controlled growth of the nuclei. To identify the nucleation mechanism, the experimental current transients were compared with those obtained using theoretical models. The Scharifker and Hills (SH) model is largely used to identify the nucleation mechanism of metal electrodeposition.[9] This model was developed from the following nucleation law (Equation 1)

$$N = N_0[1 - e^{-at}] \quad (1)$$

It is assumed that "a" should be constant for all the active sites of the electrode; i.e. the electrode surface is effectively energetically frozen. Further, this model includes Avirami's theorem, in which hemispherical diffusion to the hemispherical nuclei is considered by relating the radial flux density through the real diffusion zones to an equivalent projected diffusive flux to an electrode area.[10,11] This model considers only two limiting cases of nucleation and growth; viz. (i) instantaneous nucleation, when all the nuclei are immediately created at high nucleation rate and the number of nuclei remains constant during the growth process and (ii) progressive nucleation, when new nuclei are continuously formed at low nucleation rate during the whole process of deposition. The theoretical curves for instantaneous and progressive nucleation can be obtained by following the equations 2 and 3, respectively.

$$\left[\frac{j}{j_m}\right]^2 = 1.9542\left(\frac{t}{t_m}\right)\left[1 - \exp(-1.2564\left(\frac{t}{t_m}\right)\right]^2 \quad (2)$$

$$\left[\frac{j}{j_m}\right]^2 = 1.2254\left(\frac{t}{t_m}\right)\left[1 - \exp\ (-2.3367\left(\frac{t}{t_m}\right)^2\right]^2 \quad (3)$$

Several efforts have been made to eliminate the analysis of two separate cases by establishing a general model of electrochemical nucleation. Three general models namely Scharifker and Mostany (SM);[12] Sluyters-Rehbach, Wijenberg, Bosco and Sluyters (SRWBS)[13] and Heerman and Tarallo (HT)[14] have been employed in the literature. They have been established from the same nucleation law and Avirami's theorem used in the SH model, but with different assumptions on the thickness of the diffusion layer around the nuclei. The major assumptions and related equations of these models are given in Table 1.

(Table 1 will be placed here)

The genetic algorithm, a useful stochastic approach, has been earlier used to get the values of D, N_0 and "a" by fitting a portion of the experimental current transient with SM model.[15] The present paper aims to understand the influence of TBA^+ ions on the electrocrystallization of silver by evaluating j_0, τ, D, N_0 and "a" by fitting the experimentally obtained current transients with the calculated current transients using hybrid genetic algorithm (HGA). The theoretical currents were calculated from the SM, SRWBS and HT models. The design intention of the hybrid algorithm is to exert fully the random search ability of the genetic algorithm (GA) to provide good initial estimates of parameters for the nonlinear regression by Levenberg-Marquardt algorithms (LMA). The calculated parameters i.e. D, N_S and aN_0 obtained from the fittings were used in the principal component analysis (PCA) to examine the existence of correlation, if any, among the SH, SM, SRWBS and HT models. This paper has dual objectives; (1) understanding of the influence of a surface protecting agent during the electrosynthesis of metal nanoparticles and (2) calculation of the electrocrystallization parameters through HGA by fitting the complete chronoamperometric current transient with the electrocryatallization models, (3) evaluation of the statistical correlation among the existing electrocrystallization models for estimating electrocrystallization parameters.

2. Experimental

2.1 Chemicals and Solutions

Silver nitrate ($AgNO_3$), potassium nitrate (KNO_3), Methanol (MeOH) and tetrabutylammonium tetrafluoroborate ($TBABF_4$, 99%) used were of AR grade and were used without further purification. Millipore-MilliQ water (18.2 MΩ cm) with 10% MeOH was used to prepare working solutions. Compositions of the working solutions were (i) 10 mM $AgNO_3$+ 0.1 M KNO_3 and (ii) 10 mM $AgNO_3$ + 0.1 M KNO_3 + $TBABF_4$ (saturated) [The excess solid residue of $TBABF_4$ was filtered out].

2.2 Electrochemical Experiments

Electrochemical experiments were carried out at room temperature with Autolab PGSTAT-30 electrochemical workstation controlled by GPES software by employing a three electrode voltammetric cell having glassy carbon (GC) working electrode (area = 0.071 cm^2), platinum wire counter electrode and Hg/Hg_2SO_4 (saturated) reference electrode [$E_{Hg/Hg2SO4\ (sat'd)}$ = 0.64 V vs. Standard Hydrogen Electrode]. All the potentials are reported with respect to Hg/Hg_2SO_4 (saturated) reference electrode. Electrochemical experiments were performed after purging the working solution with high purity nitrogen for a minimum duration of 15 minutes.

2.3 Deduction of fitting parameters

The global minima of the optimisation of the electrocrystallization parameters viz. j_0, τ, D, N_0 and "a" were found out through HGA by fitting the experimentally obtained complete potentiostatic current transients with the calculated current transients from SM, SRWBS and HT models. The home built code was used for GA. The deduced parameters were finally optimized by Origin software using LMA. The optimised values obtained from GA were taken as the initial guess values in LMA. The brief descriptions of implementation of GA and LMA are given below:

2.3.1 Initialization of the population

The population is made up of individuals or chromosomes by analogy with genetics. Each individual is a code of the parameters (j_0, τ, D, N_0 and a) in a particular model and represents a trial solution to the fitting model. The initial population is randomly generated with distribution over the entire search region and is therefore less likely to become trapped in any local optima. In our studies, we have set the size of population (n) to 100. The search of j_0, τ, D, N_0 and "a" were

defined within the physical relevant range of [1×10^{-4}, 5×10^{-2}], [0.1, 400], [1×10^{-6}, 1×10^{-3}], [1×10^{3}, 5×10^{7}], [0.1, 1000], respectively.

2.3.2 Evaluation of the fitness

The fitness of an individual will be determined by the value of the residue (R). The experimental current transient contains m data points denoted as (j_i, t_i) (i = 1 to 2000). The individual population, p_k (k = 1 to n) also contains m data points denoted as (J_i, t_i) (i = 1 to 2000). The residue is calculated by the equations 12 and 13 given below:

$$\boldsymbol{j_{av}} = \sum_{i=1}^{m} \frac{j_i}{m} \quad (12)$$

$$\boldsymbol{R} = \frac{\sum_{i=1}^{m}(j_i - J_i)^2}{\sum_{i=1}^{m}(j_i - j_{av})^2} \quad (13)$$

The lower the value of R, better is the individual.

2.3.3 Genetic operation

The genetic operation allows the good fitness of the first generation to survive in the next generation. Two operators viz. Crossover and Mutation are used for the genetic operation. Crossover operator combines the parameters from two parents to create two children. Mutation operator randomly alters one or more of the parameter(s) of a single individual randomly chosen from the population. Mutation adds random changes in the new generation and removes hereditary faults of the initial population.

2.3.4 Sorting and replacement of population

The individuals in the old and new populations are sorted according to their fitness values, and better "n" individuals are selected for the population in the next generation. The genetic operations were carried out over 500 generations for arriving at the best individuals.

2.3.5 LMA algorithm

The best individuals obtained from GA were used as the initial guess values for LMA and for this purpose; we adopted the standard LMA in built in Origin software for this process.

2.4 Principal component analysis (PCA)

PCA is a way of reducing the dimensions of a large data matrix without losing the importance of any data. The principle behind the PCA is that the multivariate data can be decomposed by linear projections onto a new co-ordinate system. The new axes, known as principal components (PCs), are orientated so that the first PC (PC1) captures the largest amount of common variance. The next PC (PC2) is orthogonal to the first PC and it captures the second largest amount of common variance in its direction. The PCA was carried out by home built code.

2.5 Atomic Force Microscopy (AFM)

The AgNPs were deposited at -0.300 V for 10 s for in the absence and presence of $TBABF_4$ for inspecting the actual nuclei densities of AgNPs. The characterisation was performed by AFM (Nanosurf Easyscan 2) by scanning the area (5 µm × 5 µm) with a silicon tip (CONTR-10) in contact static mode.

3. Results and Discussion

Fig. 1 shows cyclic voltammograms of 10 mM $AgNO_3$ + 0.1 M KNO_3 on GC in (i) absence and (ii) presence of $TBABF_4$ at a scan rate of 10 mV s^{-1}. In the absence of $TBABF_4$, the cathodic and anodic peaks of silver were observed at -0.043 V and 0.159 V, respectively. However, the cathodic peak shifted to more negative potential (-0.2 V) in the presence of $TBABF_4$ and anodic peak potential did not change much. Both the cathodic and the anodic peak currents decreased significantly. The reduction of silver in the presence of $TBABF_4$ initiated at higher overpotential of ~ -0.043 V and this suggests that the cathodic reaction of Ag(I) in presence of TBA^+ ions might be governed by the charge transfer polarization.

The electrocrystallization and more precisely, the nucleation and growth of silver were investigated by chronoamperometry in the (a) absence and the (b) presence of $TBABF_4$ at selective constant potentials i.e. (i) -0.300, (ii) -0.200, (iii) -0.100 and (iv) -0.043 V (**Fig. 2**). These potentials were selected to represent the domain of concentration polarization for the cathodic reduction of Ag(I) in the absence of $TBABF_4$; and at the same time, they would represent the domains of nucleation, charge transfer polarization and concentration polarization in the presence of $TBABF_4$. Each of the chronoamperomertic current transients (**Fig. 2**) typically represents the three dimensional multiple nucleation and diffusion controlled growth of metal on GC. The initial current decreased significantly at time scales 5-300 ms. In the succeeding part of the transient, the current increased with time and passed through a maximum value followed by a steady decrease. The time constant ($1/\tau$) for the rearrangement of electrolyte species (ions/molecules) at the electrode-electrolyte interface would be observed within 1 ms. In our experiment, the current transients exhibit the time constants in the range 5-300 ms, which is relatively longer and this may be attributed to the parallel formation of adions or adatoms in addition to the nucleation and growth by direct attachment.[16] The subsequent rise in current corresponds to the increase in the overall electroactive area due to increase(s) in the number of nuclei and/or size of nuclei. The spherical diffusion zone around each nucleus grows with time. At the time corresponding to the current maxima, the spherical diffusion zones overlap and mass transfer becomes linear. The change in diffusion regime leads to a decrease in the current with increasing time obeying Cottrell equation. At -0.300 V, the j_m at time t_m was 12.6 mA cm^{-2} at 67.3 ms (**Fig. 2a(i)**) and 3.4 mA cm^{-2} at 692.0 ms (**Fig. 2b(i)**) in the absence and the presence of $TBABF_4$, respectively. It suggests that the increase in the electroactive area was suppressed as well as overlapping of the spherical diffusion zones became sluggish in the presence of $TBABF_4$. It should be noted that no current maximum was observed for sufficient time (15 s) in the potentiostatic current transient at -0.043 V in the presence of $TBABF_4$ (**Fig. 2b(iv)**); whereas j_m of 2.1 mA cm^{-2} was observed at t_m 1.55 s at the same potential in the absence of $TBABF_4$ (**Fig. 2a(iv)**). It indicates that the time period for the introduction of nucleation on GC was prolonged in presence of $TBABF_4$.

The three dimensional multiple nucleation and diffusion controlled growth was studied by Scharifker and Hills (SH) model for two limiting cases viz. instantaneous and progressive nucleations.[17-20] The dimensionless variables, $(j/j_m)^2$ vs. t/t_m obtained from the experimental current transients were plotted

with the theoretical curves for instantaneous and progressive nucleations (Fig. 3). In the absence of $TBABF_4$, the experimental curves for all applied potentials were observed in between the two limiting cases of SH-model (Fig. 3a). In the presence of $TBABF_4$, these curves became closer to the progressive type of nucleation (Fig. 3b). The nucleation parameters viz. D, aN_0, N_S were calculated for progressive type of nucleation (Equations 14-16)(Table 2).

$$j_m^2 t_m = 0.2598D(zFC)^2 \quad (14)$$

$$Mod[j_m] = 0.4615zFCD^{\frac{3}{4}}(k'aN_0)^{\frac{1}{4}} \quad (15)$$

$$N_S = \sqrt{\frac{aN_0}{2k'D}} \quad (16)$$

(Table 2 will be placed here)

The average values of D in the absence and presence of $TBABF_4$ are 3.2×10^{-5} and 3.1×10^{-5} cm^2 s^{-1}, respectively. Therefore, the presence of $TBABF_4$ did not affect the diffusion controlled growth of the silver nuclei. However, the aN_0 and N_S significantly decreased with decrease in the applied overpotential. It suggests that the electrocrystallization of silver nuclei was governed by the activation overpotential. As the overpotential increases, more and more substrate sites become active at the electrode-electrolyte interface for transferring electrons to Ag^+ ions. It is interesting to note that the number of active substrate sites as well as aN_0 decreased drastically in the presence of $TBABF_4$ at the same overpotential. This is attributed to increase in the activation overpotential for electrocrystallization of silver in the presence of $TBABF_4$. The activation polarization could be evaluated in terms of two parameters viz. "a" and N_0. However, evaluation of these two parameters separately for each transient was not possible by SH model. Further, the accuracy of the values of D, aN_0 and N_S can not be ascertained because of a single point (t_m, j_m) measurement. It also should be emphasized that the actual nucleation and growth, as evidenced in Fig. 3, did not belong to two extreme cases. Therefore, SH model does not represent the actual electrocrystallization mechanism. Subsequently, we tried to evaluate all the parameters (viz. j_0, τ, D, N_0 and a) of electrocrystallization of silver from each transient by fitting the entire curve (for the first time, the double layer discharge region was also considered in the fitting of electrocrystallization model) with a suitable nucleation model. It is important to mention that the potentiostatic current transients fitted well by HGA with all the three models with residual sum of squares ($\sim10^{-7}$) and reduced χ^2($\sim10^{-10}$) (Fig. 4). The values of five parameters obtained from three models for all the potentiostatic current transients are shown in Fig. 5. It can be seen that the values of j_0 and τ increased while N_0 and "a" decreased significantly at all potentiostatic transients in presence of $TBABF_4$. The values of D remained unaffected by the presence of $TBABF_4$. It was earlier reported that SM and SRWBS theories accurately fitted and yielded nearly equal values for N_0.[21] However, the initial fall of current was ignored in those calculations. In contrast, we considered the complete experimental current transient for the fitting purpose. Therefore, the parallel formation of adions or adatoms during the initial fall of current was considered in our calculations. Hence, a diverse values of N_0 and "a" were calculated by different models for the same current transient.

It is known that j_0 and τ are inversely proportional to the resistance of the electrolyte solution, thus they increased upon addition of $TBABF_4$ in the electrolyte. The TBA^+ ions in the bulk electrolyte do not affect the diffusion of Ag_{aq}^+ ions in the solution. However, TBA^+ ions compete with Ag_{aq}^+ ions to occupy the active sites on the electrode at negative potentials. Moreover, the adsorption of TBA^+ ions onto the electrode surface blocks the active sites as well as introduces their electrostatic interaction with the Ag_{aq}^+ ions. Therefore, the kinetics of electrocrystallization and subsequently the number of nuclei decreases in presence of TBA^+ ions. The schematic representations of the difference of electrocrystallization in the absence and presence of TBA^+ ions are shown in Fig. 6.

As we discussed earlier, the accurate fits for each current transient were obtained for SM, SRWBS and HT models. However, for same current transient, the values of j_0, τ, N_0 and "a" differed from model to model. The variation in the values of N_0 and "a" are quite significant. Similar observations were also reported elsewhere.[21,22] We considered it worthwhile to perform a statistical analysis using PCA for SH, SM, SRWBS and HT models with the values given in Table 3.

(Table 3 will be placed here)

Fig. 7 shows the distribution of SH, SM, SRWBS and HT models on PC1 vs. PC2 in the (a) absence and (b) presence of $TBABF_4$. It can clearly be seen that the four models are devoid of any correlation due to dispersion in the values of the important parameters such as N_0 and "a". Further, Fig. 8(a) shows the AFM topography (5 μm × 5 μm) of the AgNPs deposited at -0.300 V for 10 s in the absence of $TBABF_4$. The approximate density of nuclei (N_0) was found to be 2.8×10^9 cm^{-2}, which is much underestimated by SM ($\sim3.0\times10^6$ cm^{-2}), SRWBS ($\sim3.6\times10^6$ cm^{-2}) and HT ($\sim3.4\times10^6$ cm^{-2}) models. Similar result was observed for the AFM topography (5 μm × 5 μm) of the AgNPs deposited at -0.300 V for 10 s in the presence of $TBABF_4$ (Fig. 8(b)). The approximate density of nuclei was found to be 5.1×10^8 cm^{-2}, which is much underestimated by SM ($\sim1.3\times10^6$ cm^{-2}), SRWBS ($\sim8.1\times10^5$ cm^{-2}) and HT ($\sim5.4\times10^5$ cm^{-2}) models. Although the calculated values are far from the reality, the significant decrease in the number of nuclei was also observed in the presence of $TBABF_4$ and it supports the former discussions. There are a few reports which similarly observed higher nuclei density by scanning electron microscope than those calculated from the models[23-26] and no attempt was made to evaluate the value of N_0 for other cases. We note that, in the presence of $TBABF_4$, the particle size (in XY-direction) increases while it decreases along the Z-direction. The exact reason of this is not known at present and it will be explored in more details in the future. Further, the GC electrode, polished to mirror finish, inherently contains scratches of a few nano- to micro-meter width. The interfacial Gibbs energy of these scratches would be much more than the planes of GC. Therefore, more number of nuclei are located around the scratches (Fig. 8). It also supports that the assumption of constant nucleation rate is not valid in the reality of electrochemical nucleation.[27-30] Thus the higher rate of nucleation at the scratches can lead to higher number of nuclei around them. However, we note that the microscopic picture of the small segment of the electrode may not give the true quantitative nuclei density of the entire GC surface because of (1) dispersion in the particle size, (2) overlaps between the neighbouring nuclei and (3) cluster formation around the scratches.

Based on the above statistical analysis of data and the absence of any correlation among the different models, the following observations can be made. (1) The researchers should be careful in attaching any extra significance to the numerical values of j_0, τ, D, N_0, "a" of any system only based on the quality of fitting. (2) The true density of nuclei significantly differs from the calculated values from the models. (3) The compatibility of the realistic nucleation and growth mechanism with the (a) nucleation rate law (equation 1) along with the assumption of the constant nucleation rate, (b) assumptions of the diffusion zones[31-33] and (c) the compatibility of the Avirami's theory should be revaluated. The present study, therefore, corroborates the need to revise electrochemical nucleation and growth.[20,34]

Conclusions

The above study shows that the electrocrystallization of silver nuclei in presence of TBA^+ ions is governed by the activation overpotential. The TBA^+ ions in the bulk electrolyte do not affect the diffusion of Ag_{aq}^+ ions in the solution. However, TBA^+ ions compete with Ag_{aq}^+ ions to occupy the active sites on the electrode at negative potentials. Moreover, the adsorption of TBA^+ ions onto the electrode surface blocked the active sites as well as introduced, to some extent, an electrostatic interaction with the Ag_{aq}^+ ions. Therefore, the kinetics of electrocrystallization and subsequently the number of nuclei decreased in presence of TBA^+ ions. The PCA showed that the SH, SM, SRWBS and HT models do not correlate among themselves; though these four models were originated from the same nucleation law of electrocrystallization and Avirami's theorem with different arguments, which make physical senses.

List of symbols

t	: Time since the potential was applied (s)
N_0	: Number of active sites (cm^{-2})
Ns	: Saturation nucleus density (cm^{-2})
a	: Nucleation rate constant (s^{-1})
aN_0	: Effective nucleation rate (cm^{-2} s^{-1})
j	: Current density of the transient (A cm^{-2})
j_0	: Initial current density (A cm^{-2})
j_m	: Maximum current density of the transient (A cm^{-2})
t_m	: Time corresponding to j_m (s)
D	: Diffusion coefficient (cm^2 s^{-1}) of Ag(I)
τ	: Decay constant (s^{-1})
j_i	: Experimental current density at time t_i
J_i	: Calculated current density at time t_i
C	: Concentration of metal ions (mol L^{-1})
F	: Faraday's constant (96487 C mol^{-1})

Notes and references

[a] *Fuel Chemistry Division, Bhabha Atomic Research Centre, Trombay, Mumbai-400 085, India. Fax: +91-22-2550-5151; Tel: +91-22-2559-3740; E-mail: skaggr2002@rediffmail.com*

1. T. Zhang, Y.-J. Song, X.-Y. Zhang and J.-Y. Wu, *Sensors*, 2014, **14** 5860.
2. C.M. Cobley, S.E. Skrabalak, D.J. Campbell, Y. Xia, *Plasmonics*, 2009, **4**, 171.
3. P.C. Ray, *Chem. Rev.*, 2010, **110**, 5332.
4. B. Pietrobon, V. Kitaev, *Chem. Mater.*, 2008, **20**, 5186.
5. Z.M. Sui, X. Chen, L.Y. Wang, L.M. Xu, W.C. Zhuang, Y.C. Chai, C.J. Yang, *Physica E*, 2006, **33**, 308.
6. S.K. Guin, H.S. Sharma, S.K. Aggarwal, *Electrochim. Acta*, 2010, **55**, 1245.
7. S.K. Guin, J.S. Pillai, A.S. Ambolikar, A. Saha, S.K. Aggarwal, *RSC Adv.*, 2013, **3**, 17977.
8. M.E. Hyde, R.G. Compton, *J. Electroanal. Chem.*, 2003, **549**, 1.
9. B. Scharifker, G. Hills, *Electrochim. Acta*, 1983, **28**, 879.
10. M. Avrami, *J. Chem. Phys.*, 1939, **7**, 1103.
11. M. Avrami, *J. Chem. Phys.,* 1940, **8**, 212.
12. B. Scharifker, J. Mostany, *J. Electroanal. Chem.*, 1984, **177**, 13.
13. M. Sluyters-Rehbach, J.H.O.J. Wijenberg, E. Bosco, J.H. Sluyters, *J. Electroanal. Chem.*, 1987, **236**, 1.
14. (a) L. Heerman, A. Tarallo, *J. Electroanal. Chem.*, 1999, **470**, 70. (b) L. Heerman, A. Tarallo, *J. Electroanal. Chem.*, 1998, **451**, 101. (c) M. Arbib, B. Zhang, V. Lazarov, D. Stoychev, A. Milchev, C. Buess-Herman, *J. Electroanal. Chem.*, 2001, **510**, 67.
15. J. Yu, H. Cao, Y. Chen, L. Kang, H. Yang, *J. Electroanal. Chem.*, 1999, **474**, 69.
16. A. Radisic, F.M. Ross, P.C. Searson, *J. Phys. Chem. B,* 2006, **110**, 7862.
17. A.G. Oshchepkov, A.N. Simonov, P.A. Simonov, A.N. Shmakov, N.A. Rudina, A.V. Ishchenko, O.V. Cherstiouk, V.N. Parmon, *J. Electroanal. Chem.*, 2014, **729**, 34.
18. J. Xu, G. Yu, B. Hu, J. Zhang, Q. Dong, X.Y. Zhang, *Powder Technol.*, 2014, **264**, 561.
19. R.-W. Tsai, Y.-T. Hsieh, P.-Y. Chen, I.-W. Sun, *Electrochim. Acta*, 2014, **137**, 49.
20. M. Rezaei, S.H. Tabaian, D.F. Haghshenas, *Electrochim. Acta*, 2013, **87**, 381.
21. B. Scharifker, J. Mostany, M. Palomar-Pardave, I. Gonzalez, *J. Electrochem. Soc.*, 1999, **146**, 1005.
22. O. Brylev, L. Roué, D. Bélanger, *J. Electroanal. Chem.*, 2005, **581**, 22.
23. S. Salomé, N.M. Pereira, E.S. Ferreira, C.M. Pereira, A.F. Silva, *J. Electroanal. Chem.*, 2013, **703**, 80.
24. S. Langerock, L. Heerman, *J. Electrochem. Soc.*, 2004, **151**, C155.
25. F. Gloaguen, J.M. Leger, C. Lamy, A. Marmann, U. Stimming, R. Vogel, *Electrochim. Acta*, 1999, **44**, 1805.
26. A.O. Simm, X. Ji, C.E. Banks, M.E. Hyde, R.G. Compton, *ChemPhysChem*, 2006, **7**, 704-709.
27. S. Fletcher, *J. Electroanal. Chem.*, 2002, **530**, 105.
28. S. Fletcher, *J. Electroanal. Chem.*, 2002, **530**, 119.
29. R.L. Deutscher, S. Fletcher, *J. Electroanal. Chem.*, 1988, **239**, 17.
30. R.L. Deutscher, S. Fletcher, *J. Electroanal. Chem.*, 1990, **277**, 1.
31. A. Milchev, *J. Electroanal. Chem.*, 1998, **457**, 35.
32. A. Milchev, W.S. Kruijt, M. Sluyters-Rehbach, J.H. Sluyters, *J. Electroanal. Chem.*, 1993, **362**, 21.
33. W.S. Kruijt, M. Sluyters-Rehbach, J.H. Sluyters, A. Milchev, *J. Electroanal. Chem.*, 1994, **371**, 13.
34. H.J. Ustarroz, X. Ke, A. Hubin, S. Bals, H. Terryn, J. Phys. Chem. C, 2012, **116**, 2322.

Table 1 The equations and assumptions of SM, SRWBS and HT models.

Model	Equations	Assumptions	Remarks
SM	$j = j_0 \exp(-\tau t) + \frac{zFCD^{\frac{1}{2}}}{\sqrt{(\pi t)}}[1 - \exp(-N_0 \pi k' D\theta t)]$ (4) $\theta = 1 - \left[\frac{1-\exp(-at)}{at}\right]$ (5) $k' = \frac{4}{3}\sqrt{\frac{8\pi CM}{\rho}}$ (6) For silver, M =107.87 g mol^{-1} and ρ = 10.49 g cm^{-3}.	The time dependent radius of the circular projected diffusion zone around a nucleus was calculated from the time of birth of that nucleus.	It underestimates the current in the Cottrell limit.
SRWBS	$j = j_0 \exp(-\tau t) + \frac{zFCD^{\frac{1}{2}}}{\sqrt{(\pi t)}}[1 - \exp(-N_0 \pi k' D\varphi t)]$ (7) $\varphi = 1 - \left[\frac{e^{-at}}{\sqrt{(at)}} \int_0^{\sqrt{(at)}} e^{\lambda^2}\, d\lambda\right]$ (8) $\varphi = 1 - \frac{1}{\sqrt{(at)}}\left[\frac{0.051314213+0.47910725\sqrt{(at)}}{1-1.2068142\sqrt{(at)}+ 1.185724(at)}\right]$ (9)*	The planar diffusion zones of uniform thickness resulting in uniform concentration gradients over the substrate surface.	It overestimates the fractional surface coverage on the electrode.
HT	$j = j_0 \exp(-\tau t) + \frac{zFCD^{\frac{1}{2}}}{\sqrt{(\pi t)}}\left[\frac{\varphi}{\theta}\right][1 - \exp(-N_0 \pi k' D\theta t)]$ (10) $\frac{\varphi}{\theta} = \frac{\left[0.520893(at) - 1.206814(at)^{\frac{3}{4}} + 1.185724(at)^2 - 0.051314\sqrt{(at)}\right]}{\left[\{at-1+\exp(-at)\}\{1-1.206814\sqrt{(at)}+ 1.185724(at)\}\right]}$ (11)*	The thickness of the diffusion layer must be a function not only of time but also of the nucleation rate constant.	It underestimates the current in the Cottrell limit.

* Reproduced from Heerman et al., J. Electroanal. Chem., 451 (1998) 101-109 and Arbib et al., J. Electroanal. Chem., 510 (2001) 67-77.

Table 2 The derived values of D, aN_0 and N_S from the current transients at different potentials by following SH Model.

Potential (V)	In absence of $TBABF_4$			In presence of $TBABF_4$		
	D ($cm^2\ s^{-1}$)	**aN_0** ($cm^{-2}\ s^{-1}$)	**N_S** (cm^{-2})	**D** ($cm^2\ s^{-1}$)	**aN_0** ($cm^{-2}\ s^{-1}$)	**N_S** (cm^{-2})
-0.300	4.4×10^{-5}	1.3×10^{8}	4.7×10^{6}	3.5×10^{-5}	1.6×10^{6}	5.8×10^{5}
-0.200	3.1×10^{-5}	9.6×10^{5}	4.8×10^{5}	3.4×10^{-5}	4.6×10^{5}	3.2×10^{5}
-0.100	2.8×10^{-5}	3.7×10^{5}	3.1×10^{5}	2.5×10^{-5}	2.2×10^{4}	8.1×10^{4}
-0.043	2.4×10^{-5}	5.4×10^{4}	1.3×10^{5}	Could not be calculated because of absence of prominent current maximum		

Table 3 The values of the fitted parameters used for PCA.

Model		$D / (10^{-5}\ cm^2\ s^{-1})$			$N_S / (10^6\ cm^{-2})$			$aN_0 / (10^6\ cm^{-2}\ s^{-1})$		
		-0.3 V	**-0.2 V**	**-0.1 V**	**-0.3 V**	**-0.2 V**	**-0.1 V**	**-0.3 V**	**-0.2 V**	**-0.1 V**
In presence of $TBABF_4$	**SM**	4.40	3.60	3.60	3.60	0.610	0.190	273	3.37	0.331
	SRWBS	4.40	3.60	3.60	3.40	0.450	0.190	181	1.80	0.397
	HT	4.40	3.30	3.50	3.00	0.390	0.190	203	1.72	0.57
	SH	4.40	3.10	2.80	4.70	0.480	0.310	130	0.96	0.37
In absence of $TBABF_4$	**SM**	3.60	3.90	3.70	1.30	0.390	0.200	2.54	0.644	0.306
	SRWBS	3.60	3.90	3.80	0.810	0.340	0.034	1.90	0.602	0.039
	HT	3.40	3.60	3.70	0.540	0.290	0.035	2.33	0.716	0.042
	SH	3.50	3.40	2.50	0.580	0.320	0.081	1.60	0.46	0.022

Figures:

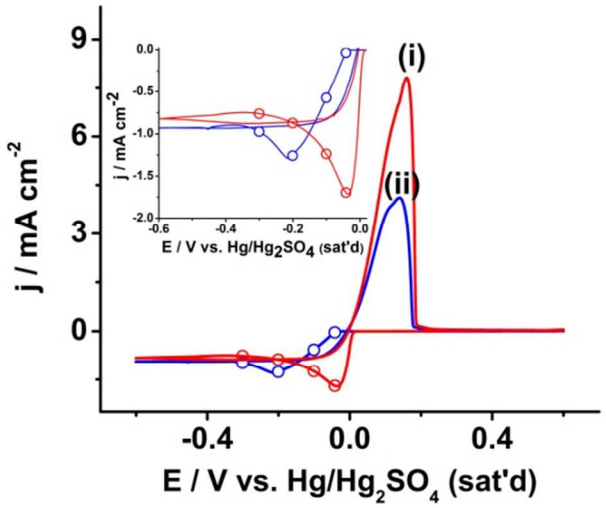

Fig. 1 Cyclic voltammograms of 10 mM $AgNO_3$ + 0.1 M KNO_3 in (i) absence and (ii) presence of $TBABF_4$ on GC at a scan rate of 10 mV s^{-1}. Inset shows the zoomed image of the cathodic peaks.

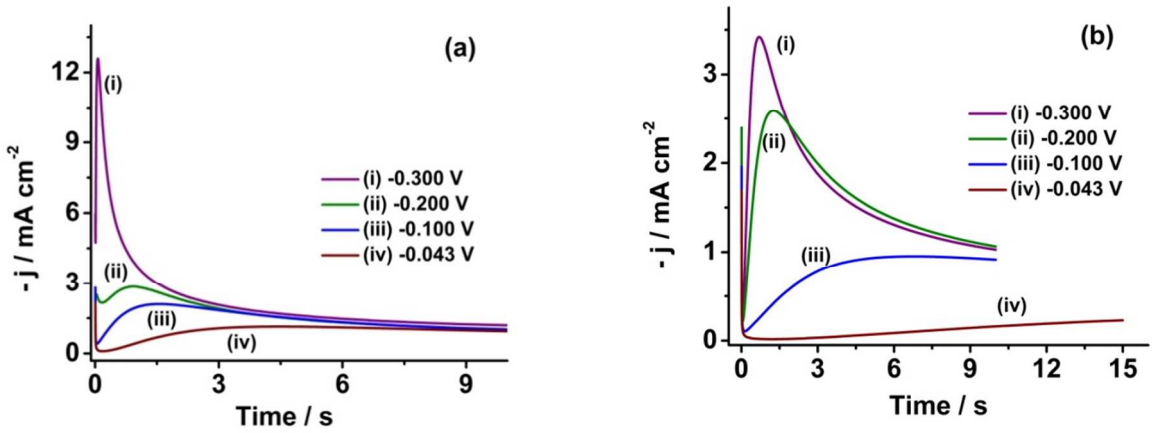

Fig. 2 The chronoamperometric current transients of 10 mM $AgNO_3$ + 0.1 M KNO_3 at (i) -0.300, (ii) -0.200, (iii) -0.100 and (iv) -0.043 V in (a) absence and (b) presence of $TBABF_4$.

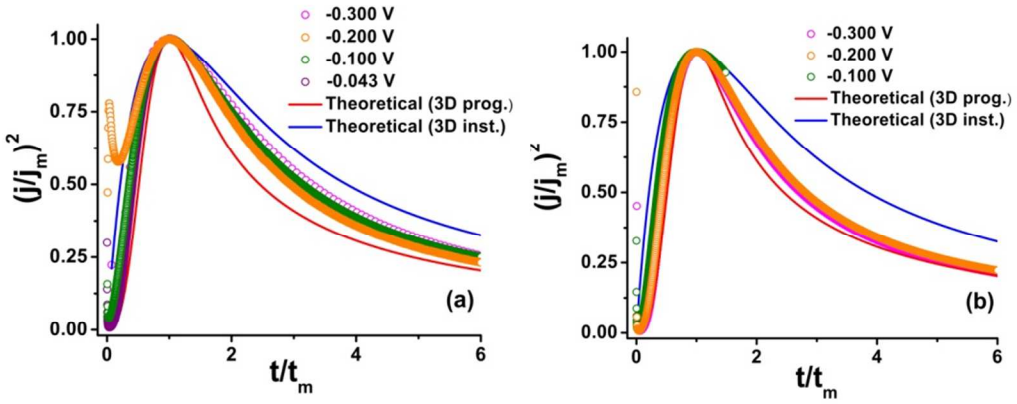

Fig. 3 The plot of dimensionless variables, $(j/j_m)^2$ vs. t/t_m obtained from the experimental current transients in the (a) absence and (b) presence of $TBABF_4$. The dimensionless variables of the calculated (theoretical) current transients for instantaneous and progressive nucleation according to the Scharifker and Hills (SH) model are also overlaid in each graph.

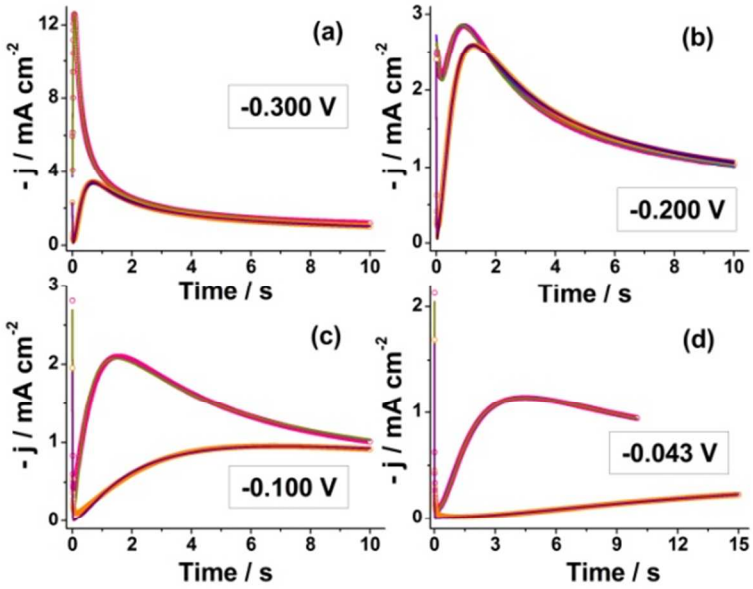

Fig. 4 The potentiostatic current transients at (a) -0.300, (b) -0.200, (c) -0.100, and (d) -0.043 V in the (i) absence (pink circles) and (ii) presence (saffron circles) of $TBABF_4$. The solid lines (colour of each line is not visible indistinguishably because of overlapping among them) are the fitted lines according to SM, SRWBS and HT models.

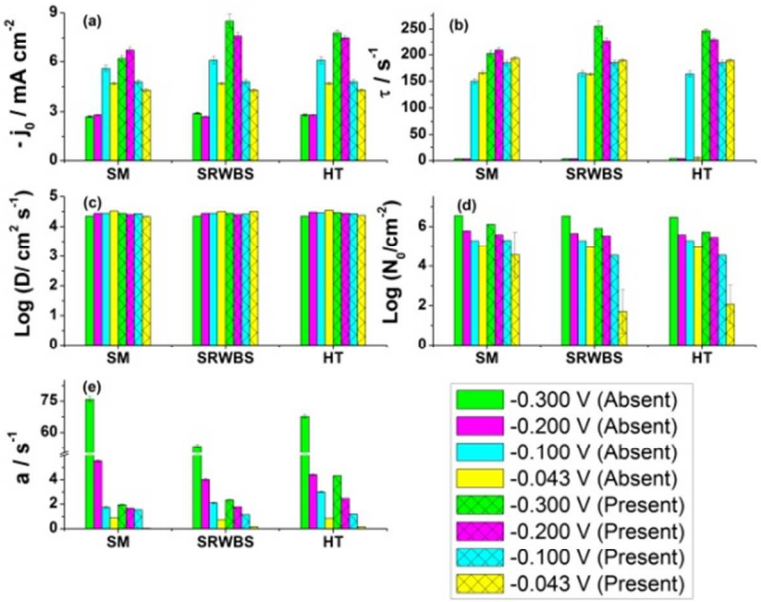

Fig. 5 The optimized fitted parameters viz. j_0, τ, Log D, Log N and "a" obtained by fitting through SM, SRWBS and HT models for each potentiostatic transient. Here (Absent) and (Present) represent the absence and presence of $TBABF_4$, respectively.

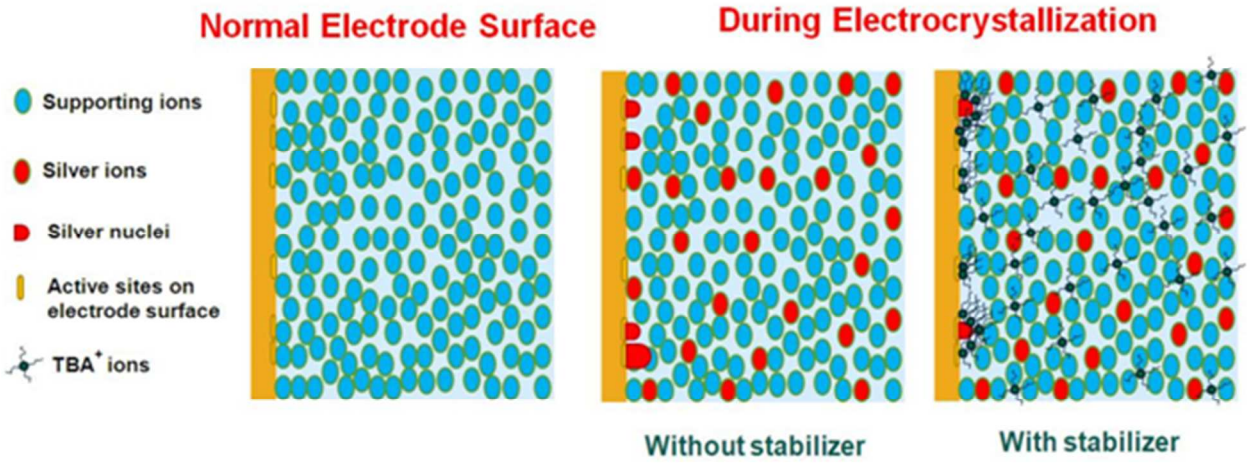

Fig. 6 Schematic representation of the difference of electrocrystallization in the absence and presence of TBA^+ ions.

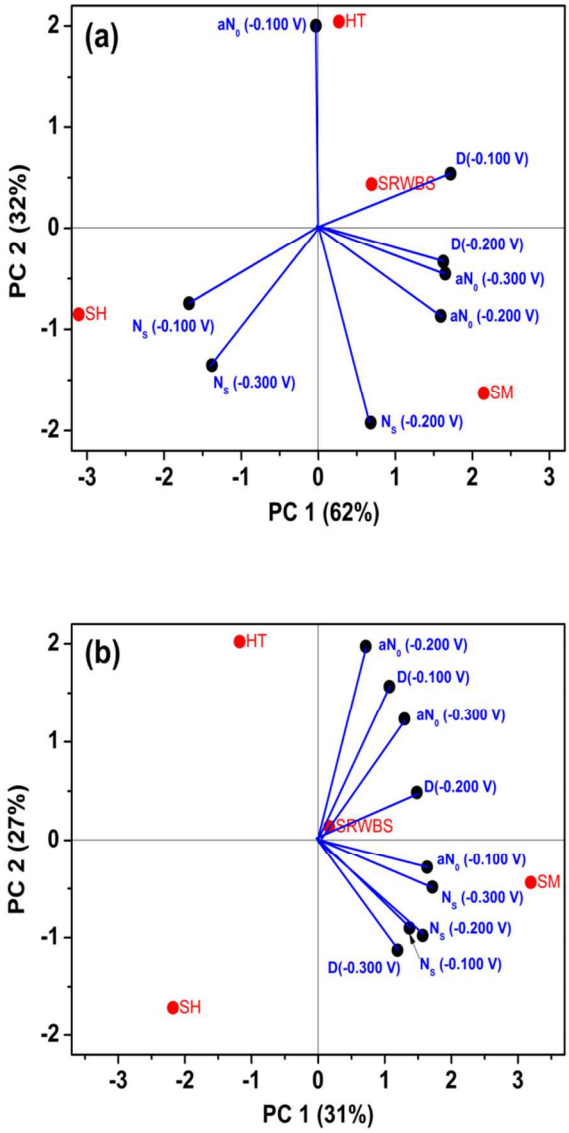

Fig. 7 The distribution of SH, SM, SRWBS and HT models on PC2 vs. PC1 in the (a) absence and (b) the presence of $TBABF_4$. The loading of each parameter are shown by the distance of the black points from the origin. In (a) D (-0.300 V) is not shown in the calculation because it had same values for the four models.

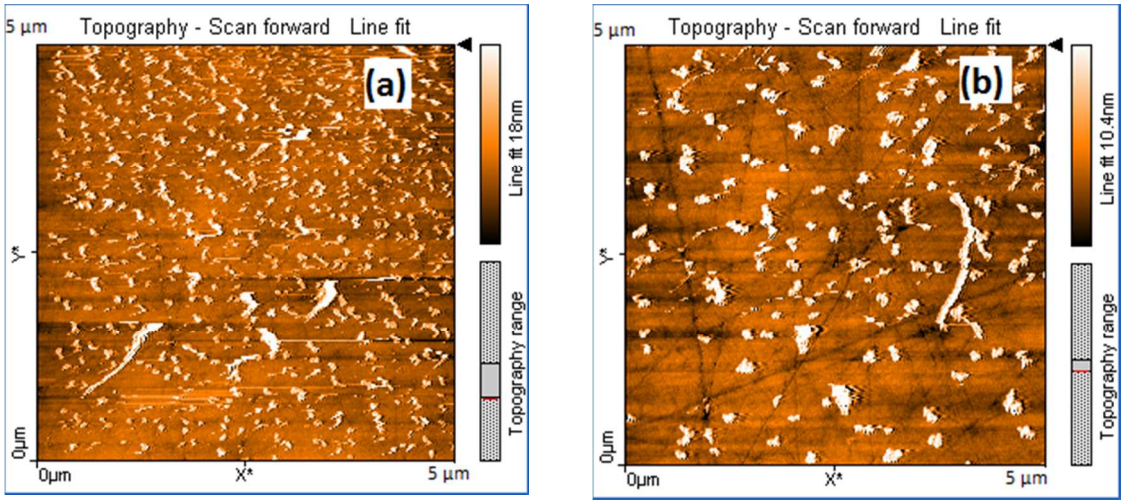

Fig. 8 The AFM topography (XY) of the AgNPs deposited on GC at -0.300 V for 10 s in (a) the absence and (b) the presence of $TBABF_4$. The vertical bar at the top right of each image represents the z-profile of the XY image.